

## DESIGN OF A WIRELESS POWER TRANSFER SYSTEM FOR HIGH POWER MOVING APPLICATIONS

Saeed Hasanzadeh and Sadegh Vaez-Zadeh \*

Center of Excellence on Applied Electromagnetic Systems and Advanced Motion Systems Research Laboratory, School of Electrical and Computer Engineering, University of Tehran, Tehran, Iran

**Abstract**—In high power applications of wireless power transfer systems as Maglev, both a high transferred power and a high efficiency are essential. However, these two requirements usually show dissimilar profiles over a range of operating conditions. Magnetic and electric models for a capacitor compensated system are used to analyze the problem. Using the analysis outcome, a compromise is made to come to an acceptable design achieving both requirements. In particular, appropriate design parameters and resonance frequency are obtained. The analytical results are confirmed by 3D FEM analysis.

### 1. INTRODUCTION

High power moving objects can be supplied economically if appropriate wireless power transfer (WPT) sources exist. A maglev system, with a linear synchronous motor, for instance, requires primary windings distributed along the track, resulting in substantial increase in the construction and maintenance cost [1,2]. Placing windings on the mover plus a proper WPT system considerably reduces the cost. A suitable structure for high power WPT systems should be designed to satisfy the best performance and meet the requirement of the application. The simplicity of the implementation is also essential in selecting the WPT structure.

In WPT for high power moving applications, the apparatus usually includes a small air gap along the main flux path that links two coils. A primary coil is located on the stationary base unit while a secondary coil is located on the vehicle. The latter coil effectively receives the power from the primary side through the air gap and

---

*Received 22 October 2012, Accepted 25 January 2013, Scheduled 28 January 2013*

\* Corresponding author: Sadegh Vaez-Zadeh (vaezs@ut.ac.ir).

delivers it to the vehicle. The power can be used immediately by a traction motors or can be stored for later use. Also, a WPT structure can be constructed in conjunction with a magnetic levitation system using Hallbach arrays [3], permanent magnets (PMs) [4], passive and self-controlled systems [5,6]. Although the required power for a levitation system is usually lower than the power needed by a propulsion system, the combined system causes a reduction in total weight of vehicle and improves its performance.

Different WPT structures for transferring high power form long primary tracks to moving objects are considered. In particular, two types of WPT systems, i.e., with long bus bars and with long magnetic material cores are proposed [7]. Also, WPT structures for monorail systems with U, S, E, Z and  $\lambda$  shapes are introduced [8]. Two WPT structures are presented and analyzed for the linear servo motors [9]. A WPT system consisting of a U shape pickup on the vehicle and three wires as primary winding is proposed for supplying movable vehicles [10]. The mentioned works not thoroughly discuss the system analysis and design, considering practical limitations such as operating frequency when both high power transfer and high efficiency are desirable. In order to attain high performances in WPT systems, capacitive compensations in both primary and secondary sides are recommended to provide resonance conditions [11]. Resonance based WPT systems save weight, space and cost of the system [12]. However, some special applications can be supplied by non-resonance based WPT systems with proper designs [13].

Coaxial WPT systems including a straight primary wire passing through the center of a cylindrical secondary core with an air gap have already been recognized. It can be used in Maglev as well as in wireless EV charging systems [14,15] and power delivery system for mining applications [16]. Also, a high power coaxial inductive power transfer pickup is presented [17]. A partial design of the system is reported recently [18]. However, a systematic modeling, analysis and design procedure is not reported in the literature.

In this work, a coaxial WPT system as in Fig. 1 is considered. A mathematical model is used for the system analysis including the compensating capacitors. The analysis includes the calculation of transferred power, efficiency, coupling coefficient, etc.. Then, a design procedure is proposed to achieve high efficiency and high transferred power. The work extends the application of low power resonance-based inductive magnetic coupling to high power applications like Maglev [19,20]. The system parameters are obtained to meet the design specifications. Analytical results are verified by 3D FEM simulations to confirm the design.

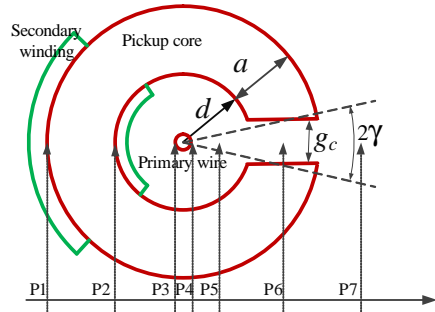
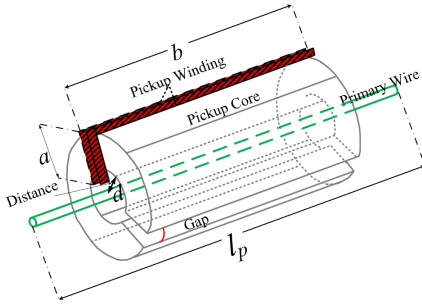


**Figure 1.** A schematic view of the gapped coaxial WPT system.

**Figure 2.** Cross section of the gapped coaxial WPT system.

## 2. WPT MODEL

A physical model of the coaxial WPT system is presented in Fig. 1, where the primary side is a straight wire supplied by a high frequency source on the ground. The secondary side consists of an open hollow cylindrical core of magnetic material and a pickup winding, all mounted on a maglev vehicle. A radial air gap takes the two sides apart.

### 2.1. Magnetic Modeling

Referring to Fig. 2, Ampere Law can be written as:

$$I_1 = \oint H \cdot dl = \varphi (\mathbb{R}_m + \mathbb{R}_g) \tag{1}$$

where,  $\mathbb{R}_m$ ,  $\mathbb{R}_g$  are the secondary core reluctance and the air gap reluctance respectively which can be calculated by a 3D model as shown in Fig. 1. The secondary flux, induced by  $I_1$ , is then obtained as:

$$\varphi \simeq \frac{\mu_0}{2\pi} \frac{ab}{(d + a/2)} \frac{\mu_r}{1 + \frac{\gamma}{\pi}(\mu_r - 1)} \ln \left( \frac{a + d}{d} \right) I_1 \tag{2}$$

where,  $a$ ,  $b$ ,  $d$ , and  $\gamma$  are shown in Figs. 1 and 2. Also,  $\gamma$  can be represented as:

$$\gamma \simeq \sin^{-1} \left( \frac{g_c}{2d + a} \right) \tag{3}$$

Comparing (2) to a linkage flux of a current carrying rectangular wire, an equivalent permeability is defined as:

$$\mu_{av} = \frac{\mu_r}{1 + \frac{\gamma}{\pi}(\mu_r - 1)} \tag{4}$$

Then, the secondary linkage flux is given by:

$$\lambda_{av} \simeq \frac{N_2 \mu_0 \mu_{av}}{2\pi} ab \frac{\ln\left(\frac{a+d}{d}\right)}{(d+a/2)} I_1 \quad (5)$$

As a result, the system mutual inductance is obtained as:

$$M \simeq \frac{N_2 \mu_0 \mu_{av}}{2\pi} ab \frac{\ln\left(\frac{a+d}{d}\right)}{(d+a/2)} \quad (6)$$

Also, Applying Ampere Law, the primary and secondary inductances are obtained respectively as:

$$L_1 \simeq \frac{\mu_0 l_p}{8\pi} \left[ 1 + \frac{1}{2} \ln\left(\frac{\sqrt{d(d+a)}}{r_1}\right) \right] \quad (7)$$

$$L_2 \simeq \frac{N_2^2 \mu_0 \mu_r ab}{\pi(2d+a) + \mu_r g_c} \quad (8)$$

where,  $l_p$ ,  $N_2$ ,  $\mu_r$  and  $r_1$  are the length of primary wire, the number of secondary turns, the relative permeability of the secondary core and the primary wire radius respectively.

## 2.2. Electric Modeling

The system is represented by the equivalent circuit of Fig. 3. The primary wire and the secondary winding are modeled by two coupled  $RL$  circuits of impedances  $R_1 + j\omega L_1$  and  $R_2 + j\omega L_2$  respectively where:

$$R_1 = \frac{\rho_{cu} J_1}{I_1} l_p \quad (9)$$

$$R_2 = \frac{\rho_{cu} J_2}{I_2} (2N_2(a+b)) \quad (10)$$

and  $J_1$ ,  $J_2$  and  $\rho_{cu}$  are the primary and secondary winding current densities and the copper resistivity respectively.

The series compensating capacitors  $C_1$  and  $C_2$ , are connected to the primary and secondary sides respectively. The capacitances are determined such that a common resonance frequency of  $\omega_0$  is provided in two sides as:

$$\omega_0 = \frac{1}{L_1 C_1} = \frac{1}{L_2 C_2} \quad (11)$$

The transferred power passing through the air gap is readily obtained from the equivalent circuit as [21]:

$$P_2 = \frac{\omega_0^2 M^2}{R_L} I_1^2 \quad (12)$$

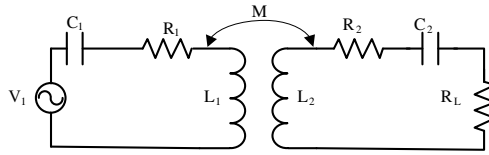


**Figure 3.** Circuit model of the coaxial WPT system.

Also, the system efficiency can be calculated as follows:

$$\eta = \frac{R_L}{R_L + R_2} \frac{1}{1 + \frac{R_1(R_L + R_2)}{\omega_0^2 M^2}} \quad (13)$$

It is proved that the maximum efficiency occurs at the resonance frequency,  $f_0$ , and the maximum power is transferred at this frequency or  $f_L$  and  $f_H$  at obtained as:

$$f_L = \frac{f_0}{\sqrt{1+k}}, \quad f_H = \frac{f_0}{\sqrt{1-k}} \quad (14)$$

where,  $k$  is the magnetic coupling coefficient given by:

$$k = \frac{M}{\sqrt{L_1 L_2}} \quad (15)$$

If the system is compensated by series capacitors, it is possible to introduce an overall coupling coefficient as [22]:

$$k_{ov} = k \left( \frac{\omega_0}{\omega} \right) \sqrt{1 + \left( \frac{\omega L_2}{R_2 + R_L} \right)^2} \quad (16)$$

A desirable frequency range, over which acceptable transferred power and efficiency are obtained, can be defined as:

$$BW = f_H - f_L \quad (17)$$

### 3. SYSTEM ANALYSIS

Using the system models presented above, a WPT system for Maglev applications is analyzed in this section where the system rated values and parameters are already known. The input and transfer powers of the system, plus the system efficiency are plotted in Fig. 4 by (12) and (13) respectively. It is seen that the input and transfer powers have similar shapes. There are two frequencies,  $f_L$  and  $f_H$ , over which the input and transfer powers reach their maximum values. The maximum transfer efficiency at the resonance frequency,  $f_0$ , located in

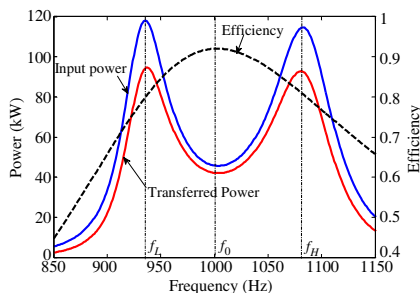


**Figure 4.** Input and transfer powers and efficiency versus frequency.

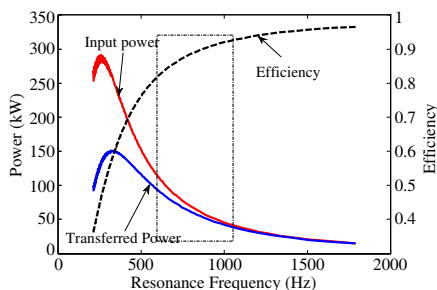


**Figure 5.** Input and transfer powers and efficiency versus resonance frequencies.

the frequency boundary of  $f_L < f_0 < f_H$ , mentioned in the previous section, is seen in Fig. 4.

The system efficiency and input and transferred power are plotted versus resonance frequencies in Fig. 5. It is seen that the transfer efficiency drops gradually with the increasing transfer power. Therefore, there is a conflict between high efficiency and high transfer power. However, in high power applications like Maglev both high efficiency and high transfer power are essential. As a result, a compromise between high efficiency and high transfer power is needed.

It is wise to consider the knee of the efficiency locus of Fig. 5 as an acceptable operating region. This is shown in Fig. 5 by a rectangular zone. Choosing a desired frequency on the acceptable region, the primary and secondary capacitances are obtained from (11) where  $L_1$  and  $L_2$  are known.

#### 4. WPT SYSTEM DESIGN

The design specifications of a system are given in Table 1. using this data, one would find  $R_L = 1.25 \Omega$ , and  $I_2 = 200$ . Also, having used (12) yields:

$$M = \frac{\sqrt{P_{out} R_L}}{\omega_0 I_1} \tag{18}$$

Choosing an appropriate current density,  $R_1$  is given by (9). Assuming that there are series resonance circuits in both sides of the system, the following relationship is held:

$$V_1 = R_1 I_1 + jM\omega I_2 \tag{19}$$

**Table 1.** Given data for system design.

Characteristics:	
Operating Frequency,	$f = 1 \text{ kHz}$
Output Power,	$P_{out} = 50 \text{ kW}$
Load Voltage,	$V_2 = 300 \text{ V}$
Primary Current,	$I_1 = 500 \text{ A}$
Copper Resistivity,	$\rho_{cu} = 2.05 * 10^{-8} \Omega\text{-m}$
Primary Length	$l_p = 200 \text{ m}$
Pickup Core Material:	
Maximum Flux Density,	$B_m = 1.4 \text{ T}$
Relative Permeability,	$\mu_r = 10^5$

Considering the system structure of Fig. 2, the air gap length,  $g_c$ , is chosen four times the radius of the primary wire,  $r_1$ , in order to prevent undesirable physical contact. As a result,  $r_1$  is obtained as:

$$r_1 = \sqrt{\frac{I_1}{\pi J_1}} \quad (20)$$

$$g_c = 4r_1 \quad (21)$$

Considering physical limitation of secondary winding, the values of  $a$  and  $d$  are obtained. The values of  $\gamma$  and  $\mu_{av}$  are then calculated from (3) and (4).

Deciding on proper values of  $b$  and  $N_2$ ,  $M$  is calculated from (18). An appropriate value for  $a$  can be regarded as  $a = b/3$ . An examination of  $M$  versus  $N_2$  and  $a$  is carried out as presented by Fig. 6 before  $N_2$  is decided. Fig. 6 shows that for a fixed length of the secondary winding wire, the less the turn number,  $N_2$ , and the higher the value of  $a$ , the larger the mutual inductance,  $M$ .

Having,  $J_2$ , it is possible to find out  $R_2$  by using (10). The value of  $r_2$  is then calculated by (20). Then  $L_1$  and  $L_2$  are calculated. Also, the compensating capacitors are determined as:

$$C_1 = \frac{1}{4\pi^2 f_0^2 L_1}, \quad C_2 = \frac{1}{4\pi^2 f_0^2 L_2} \quad (22)$$

Finally, the system efficiency is obtained by using (13). The flux density is then examined in order not to saturate so that:

$$B_m \leq \frac{M\omega I_1}{2\sqrt{2}\pi f(ab)} \quad (23)$$

It is possible to get close to a system design with good efficiency without saturation. It is achieved by choosing appropriate dimensions,

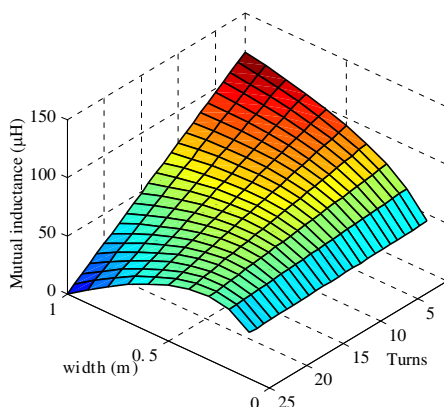


**Figure 6.** Mutual inductance versus turns and width of secondary coil.

operating frequency and current densities. Such a design presented in Table 2. It is wise to mention if the designed specifications are not met, some of the parameters are to be reconsidered. For instance, the primary and secondary current densities must be revised. This in turn changes many other parameters.

## 5. DESIGN EVALUATION

A 3D FEM analysis is carried out on a certain resonance frequency to evaluate the design. A 2D FEM cannot be used for the system analysis since the primary side is much longer than the secondary side and consists of two parts, i.e., a part coupled to the secondary side and an uncoupled part. The results of 3D FEM are illustrated in Figs. 7(a) and (b) by two and three dimensional graphs respectively. It is seen in Fig. 7(a) that high flux densities appear in and around the air gap, while the flux density in the secondary core remains limited. The magnetic flux vectors are depicted in Fig. 7(b). It is seen that the vector values are independent from the secondary core length. Also, regardless of a relative speed between the primary and secondary, end effects are not visible. This is in contrast to a linear induction machine since in this case the flux produced by the primary wire is fixed throughout the wire in every instance. While in an induction machine the flux distribution is sinusoidal.

An evaluation of flux density distribution along with a line passing through the center of primary wire and the middle of the air gap is presented in Fig. 8. The flux density, in particular, is considered at



**Table 2.** Calculated parameters of the WPT system.

Symbol	Quantity	Value
$R_L$	Load Resistance	1.8 $\Omega$
$I_2$	Secondary Current	167 A
$M$	Mutual Inductance	95.5 $\mu\text{H}$
$J_1$	Primary Current Density	$2 * 10^6$ A/m <sup>2</sup>
$R_1$	Primary Wire Resistance	0.0164 $\Omega$
$S_1$	Primary Wire Area	250 mm <sup>2</sup>
$r_1$	Radius of Primary Wire	8.92 mm
$g_c$	Gapped Distance	3.57 cm
$d$	Distance Between Two Sides	20 cm
$a$	Width of Secondary Winding	15 cm
$\gamma$	Gapped Corresponding Angle	3.72 deg
$\mu_{av}$	Equivalent Relative Permeability	48.3667
$b$	Length of Secondary Winding	45 cm
$N_2$	Turn Number of Secondary Winding	72
$J_2$	Secondary Current Density	$4 * 10^6$ A/m <sup>2</sup>
$R_2$	Secondary Resistance	0.0424 $\Omega$
$r_2$	Radius of Secondary Wire	3.64 mm
$S_2$	Secondary Wire Area	42 mm <sup>2</sup>
$R_{eq2}$	Reflected Secondary Impedance	0.1954 $\Omega$
$V_1$	Source Voltage	106 V
$L_1$	Primary Inductance	27 $\mu\text{H}$
$L_2$	Secondary Inductance	12.3 mH
$k$	Coupling Coefficient	0.167
$C_1$	Primary Capacitor	940 $\mu\text{F}$
$C_2$	Secondary Capacitor	2 $\mu\text{F}$
$\eta$	System Efficiency	90%
$B_m$	Maximum Flux Density	0.5 T

It also shows that the system efficiency is improved with an increasing resonance frequency. The figures confirm the validity of the analytical results as they are close to the FEM results. It is seen that the FEM results adopt the analytical results in the high power ratings as well. The exerted parameters in the analytical model are imported from the FEM analysis of the WPT model.

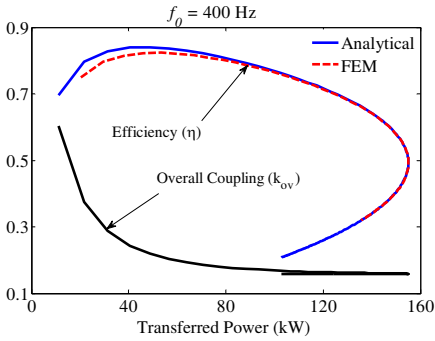


**Figure 10.** Efficiency and overall coupling coefficient versus transferred power at resonance frequency of 400 Hz.

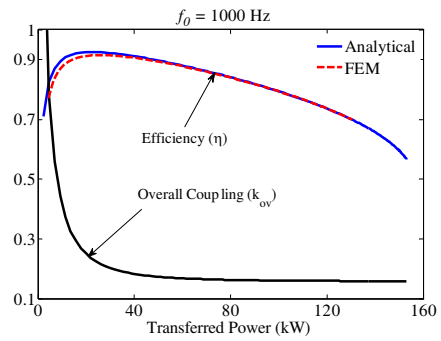


**Figure 11.** Efficiency and overall coupling coefficient versus transferred power at resonance frequency of 1000 Hz.

Figure 10 depicts the system efficiency and overall coupling coefficient versus the transferred power at a resonance frequency of 400 Hz. It is seen while the overall coupling coefficient decreases monotonically by increasing the transferred power; the system efficiency reaches a maximum of 82% before decreasing with the increasing transferred power. The same situation is repeated in Fig. 11 for a resonance frequency of 1000 Hz. In Figs. 10 and 11, a compromise between  $k_{ov}$  and transferred power can be found on the knee of  $k_{ov}$  curve where both  $k_{ov}$  and transferred power are not low. It is interesting to notice that the maximum efficiency in both frequencies almost coincides with the knee of  $k_{ov}$ . Therefore, an optimal operating point can be found for every resonance frequency at which the transferred power, system efficiency and overall coupling coefficient are acceptable.

## 6. CONCLUSIONS

Presenting magnetic and electric models for a capacitor compensated wireless power transfer system, the transfer power, the efficiency and the coupling coefficient are analyzed for a high power application. It is observed that the transferred power and efficiency versus the resonance frequency follow different trends. In fact, these two requirements couldn't be achieved at the same frequency at the first glance. In other hand, the high transferred power is obtained at a low resonance frequency but the high efficiency is achieved at a high resonance frequency. Fortunately, a compromise can be reached to achieve acceptable transferred power and high efficiency at the knee of the

coupling coefficient curve. This is done by a graphical determination of an acceptable operating region on the knee. The analytical results are verified by 3D FEM analysis. The proposed analysis and design rule can be used as a tool for more accurate system design and optimization.

## REFERENCES

1. Lee, H. W., K. C. Kim, and J. Lee, "Review of Maglev train technologies," *IEEE Trans. on Magnetics*, Vol. 42, No. 7, 1917–1925, Jul. 2006.
2. Cassat, A. and M. Jufer, "Maglev projects technology aspects and choices," *IEEE Trans. Appl. Supercond.*, Vol. 12, No. 1, 915–925, Mar. 2002.
3. Ravaud, R., G. Lemarquand, and V. Lemarquand, "Halbach structures for permanent magnets bearings," *Progress In Electromagnetic Research M*, Vol. 14, 263–277, 2010.
4. Janssen, J. L. G., J. J. H. Paulides, and E. A. Lomonova, "Study of magnetic gravity compensator topologies using an abstraction in the analytical interaction equations," *Progress In Electromagnetics Research*, Vol. 128, 75–90, 2012.
5. Matrosov, V. M., A. Musolino, R. Rizzo, and M. Tucci, "A new passive maglev system based on eddy current stabilization," *IEEE Trans. on Magnetics*, Vol. 45, No. 3, 984–987, Mar. 2009.
6. Di Puccio, F., A. Musolino, R. Rizzo, and E. Tripodi, "A self-controlled maglev system," *Progress In Electromagnetics Research M*, Vol. 26, 187–203, 2012.
7. Abel, E. and S. Third, "Contactless power transfer, an exercise in topology," *IEEE Trans. on Magnetics*, Vol. 20, No. 5, 1813–1815, 1984.
8. Elliott, G. A. J., G. A. Covic, D. Kacprzak, and J. T. Boys, "A new concept: Asymmetrical pick-ups for inductively coupled power transfer monorail systems," *IEEE Trans. on Magnetics*, Vol. 42, No. 10, 3389–3391, 2006.
9. Woo, K., H. Park, and Y. Cho, "Contactless energy transmission system for linear servo motor," *IEEE Trans. on Magnetics*, Vol. 41, No. 5, 1596–1599, 2005.
10. Sergeant, P. and A. Van den Bossche, "Inductive coupler for contactless power transmission," *IET Electric Power Applications*, Vol. 2, No. 1, 1–7, 2008.
11. Kurs, A., A. Karalis, R. Moffatt, J. D. Joannopoulos, P. Fisher, and M. Soljacic, "Wireless power transfer via strongly coupled magnetic resonances," *Science*, Vol. 317, 83–86, 2007.

12. Song, B. M., R. Kratz, and S. Gurol, "Contactless inductive power pickup system for maglev applications," *Proc. Conf. 37th IAS Ann. Meeting*, Vol. 3, 1586–1591, 2002.
13. Peng, L., O. Breinbjerg, and N. A. Mortensen, "Wireless energy transfer through non-resonant magnetic coupling," *Journal of Electromagnetic Waves and Applications*, Vol. 24, Nos. 11–12, 1587–1598, 2010.
14. Klontz, K., D. Divan, and D. Novotny, "An actively cooled 120-kW coaxial winding transformer for fast charging electric vehicles," *IEEE Transactions on Industry Applications*, Vol. 31, No. 6, 1257–1263, 1995.
15. Hasanzadeh, S., S. Vaez-zadeh, and A. H. Isfahani, "Optimization of a contactless power transfer system for electric vehicles," *IEEE Transactions on Vehicular Technology*, Vol. 61, No. 8, 3566–3573, Oct. 2012.
16. Novotny, D. W. and R. D. Lorenz, "Contactless power delivery system for mining applications," *IEEE Transactions on Industry Applications*, Vol. 3, No. 1, 1995.
17. Raabe, S., S. Member, J. T. Boys, and G. A. Covic, "A high power coaxial inductive power transfer pickup," *PESC Conf.*, Vol. 2, No. 1, 4320–4325, 2008.
18. Lastowiecki, J. and P. Staszewski, "Sliding transformer with long magnetic circuit for contact-less electrical energy delivery to mobile receivers," *IEEE Trans. on Industrial Electronics*, Vol. 53, No. 6, 1943–1948, 2006.
19. Luo, X., S. Niu, S. L. Ho, and W. N. Fu, "A design method of magnetically resonating wireless power delivery systems for bio-implantable devices," *IEEE Trans. on Magnetics*, Vol. 47, No. 10, 3833–3836, 2011.
20. Ho, S., J. Wang, W. Fu, and M. Sun, "A comparative study between novel witricity and traditional inductive magnetic coupling in wireless charging," *IEEE Trans. on Magnetics*, Vol. 47, No. 5, 1522–1525, 2011.
21. Villa, J. L., J. Sallán, A. Llombart, and J. F. Sanz, "Design of a high frequency inductively coupled power transfer system for electric vehicle battery charge," *Applied Energy*, Vol. 86, No. 3, 355–363, Mar. 2009.
22. Hasanzadeh, S. and S. Vaez-Zadeh, "Performance analysis of contactless electrical power transfer for Maglev," *Journal of Magnetics*, Vol. 17, No. 2, 115–123, Jun. 2012.